UCRL-JC-115390
PREPRINT

Rapid Thermal Processing of Steel Using High Energy Electron Beams

J. W. Elmer
M. A. Newton
A. C. Smith Jr.

This paper was prepared for submittal to the
Laser and Electron Beam in Welding, Cutting,
and Surface Treatment State of the Art 1993
5th Biannual Conference
Reno, NV
November 1-2, 1993

November 10, 1993

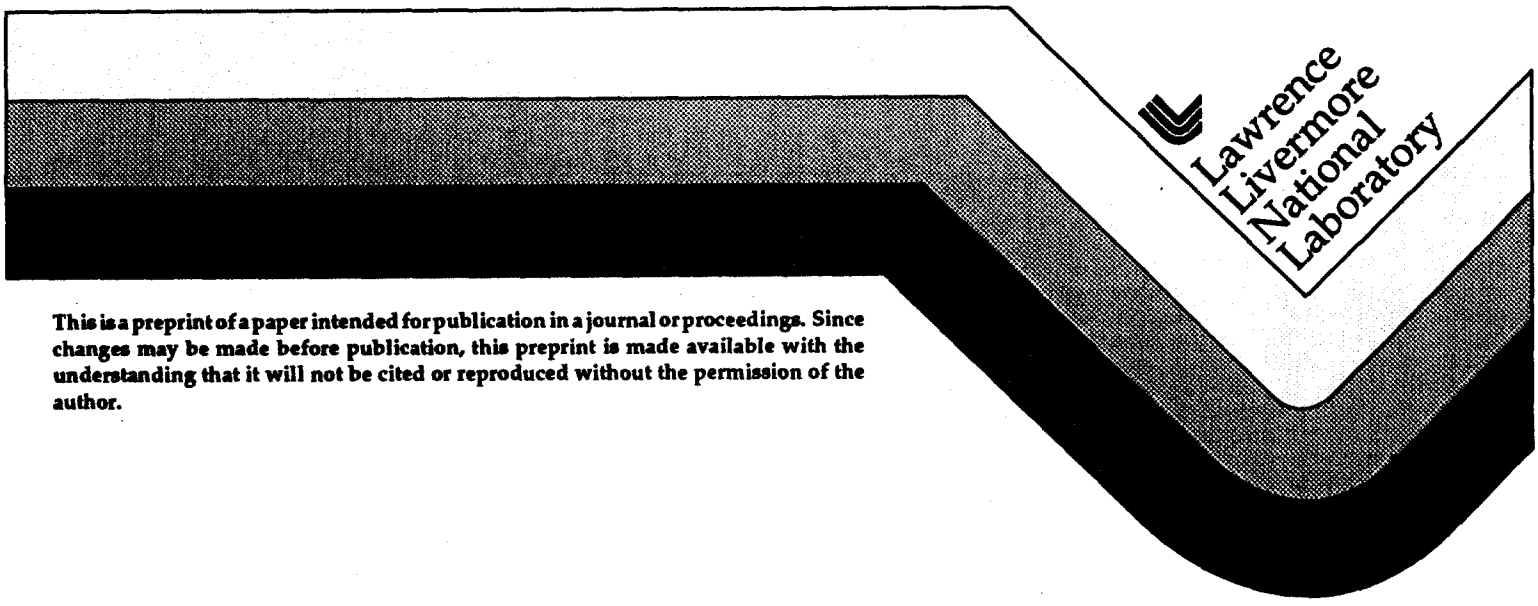

Rapid Thermal Processing of Steel Using High Energy Electron Beams

J. W. Elmer and M. A. Newton
Lawrence Livermore National Laboratory

A. C. Smith Jr.
Ballena Systems Corporation

This paper was prepared for presentation to:
The Laser and Electron Beam in Welding, Cutting and Surface Treatment State of the Art 1993, Fifth Biannual Conference, November, 1993

ABSTRACT

High energy electron beams (HEEBs) with megavolt energies represent a new generation of charged particle beams that rapidly deposit up to several hundred joules/pulse over areas on the order of a few square millimeters to 100s of square centimeters. These pulsed beams have energies in the 1 to 10 MeV range, which enables the electrons to deposit large amounts of energy deeply into the material being processed, and these beams have short pulse durations (50 ns) that can heat materials at rates as high as 10^{10} °C/s for a 1000 °C temperature rise in the material. Lower heating rates, on the order of 10^4 °C/s, can be produced by reducing the energy per pulse and distributing the total required energy over a series of sub-ms pulses, at pulse repetition frequencies (PRFs) up to several kHz. This paper presents results from materials processing experiments performed on steel with a 6 MeV electron beam, analyzes these results using a Monte Carlo transport code, and presents a first-order predictive method for estimating the peak energy deposition, temperature, and heating rate for HEEB processed steel.

INTRODUCTION

Rapid thermal processing (RTP) of materials is a field that has incorporated many innovations in new heat source technology. Many of the new RTP technologies have been applied to the processing of thin film materials where relatively small amounts of heat are deposited on the surface of the substrate and diffuse into the material in order to modify its microstructure. Isothermal processes such as thermal radiation, plasma, electrical resistance, lamps, and electron beams have been used to heat materials on the 1 to 100 s time periods; thermal flux techniques such as scanning laser and electron beams have been used to heat materials on the 1 to 100 ms time scale; and adiabatic methods such as pulsed laser and electron beams have been used to heat materials on the 1 to 1000 ns time scale [1].

The heat source requirements for RTP of thick components are substantially different than those for thin film processing. For example, larger amounts of energy are required while, at the same time, depositing the energy in a way that the material does not overheat, melt, or vaporize. These requirements can only be achieved by heat sources that pulse or scan and deposit their energy deeply into the material being processed. These characteristics can not be achieved through conventional laser or electron beam processing of thick metals or alloys. However, intense HEEBs can be used for RTP of these materials since these beams deposit energy to controllable depths at nearly instantaneous rates (nanoseconds) when compared with the thermal response time of the material [2].

This paper presents results from HEEB experiments that were conducted in order to gain an initial understanding of the physics and metallurgy of HEEB/materials interactions. These experiments investigated the beam fluence thresholds for annealing/heat-treating, melting, and vaporization of steel, and investigated the optimum conditions for deep localized heat treating of steel. The results of these experiments indicated that HEEBS have great potential for rapid/deep heating, localized hardening, and localized annealing of steel, for both stationary and moving beams at both normal incidence and glancing angles. This paper extends the results of a previous paper [3] by analyzing the HEEB/steel interaction in greater detail using Monte Carlo transport modeling of the volumetric energy deposition, in order to develop first-order predictive relations for a wide range of HEEB processing conditions.

EXPERIMENTAL PROCEDURES

Electron Accelerator

The Experimental Test Accelerator II (ETA II) at Lawrence Livermore National Laboratory (LLNL) was used to perform the experiments described in this paper. ETA II is a linear induction accelerator, capable of accelerating up to 50 pulses of a 2.5 kA electron beam at peak pulse repetition rates of 2 kHz, with each pulse having a duration of approximately 60 ns full width half maximum (FWHM). ETA II is a unique facility because it combines high brightness (~100 A/[mm-rad]^2), high electron beam currents (2.5 kA maximum) and energies in excess of 5 MeV, with high average power capability (~2 MW maximum). The focused beam can be precisely controlled using a magnetic steering system to position the beam at specific locations on the workpiece or to rapidly scan the beam across the surface of the workpiece. The total number of pulses and the repetition rate can also be easily varied to control the magnitude and rate of energy deposition into the workpiece.

The size and position of the electron beam were determined using a charged couple device camera to image the optical Cerenkov radiation emitted from a thin quartz foil placed in the beam path [4]. Once the beam was properly positioned and characterized, the quartz foil was removed and the workpiece was inserted into the beam path. Figure 1a shows a surface plot of the electron distribution in a tightly focused

beam with a diameter of 3.5 mm FWHM. Figure 1b plots the current versus time profile of a 1.2 kA/pulse, 6 MeV beam, showing the pulse duration of 60 ns FWHM. The pulse repetition frequency (PRF), defined as the frequency at which the pulses are delivered in each burst, was adjusted between 100 and 2000 Hz, and the beam current was adjusted between 0.9 kA and 1.25 kA/pulse, thus providing approximately 325-450 J/pulse. Machine operation was limited to 50 pulses in a single burst, however, bursts could be repeated approximately every minute.

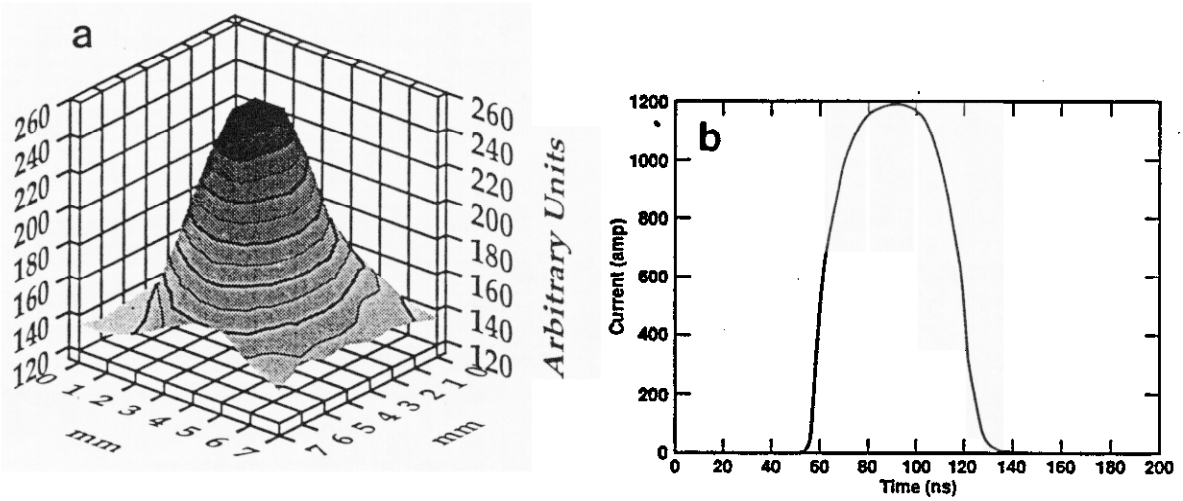

Fig. 1: a) Surface plot of the electron distribution, and b) current versus time plot of the pulse width for a 1.2 kA/pulse, 6 MeV beam.

Materials Processing and Characterization

Materials processing experiments were conducted at the end of the accelerator in an evacuated cavity with viewing ports to monitor the experiments. All experiments were performed using a 6 MeV electron beam with a vacuum of 10^{-6} torr at the workpiece location, and the electron beam pulse duration was maintained constant at 60 ns FWHM. Experiments were performed by placing 5 mm thick by 100 mm square plates in the beam line of the ETAII accelerator and processing the plates with various fluences at an acceleration voltage of 6 MeV. The effects of the beam's average power, power density, energy density, and the total energy deposited per unit area were investigated by varying the PRF, beam diameter, and number of pulses per burst.

Rapid thermal processing experiments were conducted on cold finished AISI 1018 plain carbon steel with a composition Fe, 0.16%C, 0.68%Mn, 0.12%Cr, 0.25%Si. After HEEB processing, the samples were analyzed using optical microscopy. Samples

were prepared by sectioning through the center of the processed region, and preparing the sections for optical microscopy using conventional metallographic procedures.

Monte Carlo Transport Modeling

Modeling of the HEEB energy deposition was performed using the CYLTRAN Monte Carlo transport code [5,6]. This code calculates the development of the electron/photon cascade that occurs as high energy electrons enter and interact with the material. By following the 3-dimensional particle trajectory of $2x10^4$ electron histories into an axisymmetric workpiece, enough statistics are gathered to determine the spatial deposition of the beam's energy in Joules per gram of material. Provisions are made in the code to input the composition of the workpiece and to simulate the effects of different beam radii, locations, and angles of impingement. In the calculations presented here, the energy distribution was assumed to have a "top-hat" beam profile with uniform energy over the diameter of the beam.

RESULTS AND DISCUSSION

HEEB Experiments / Monte Carlo Code Comparison

The 6 MeV ETA II beam was used to subsurface heat-treat plain carbon steel in order to experimentally verify the deep HEEB energy penetration into materials. Figure 2a shows a metallographic cross section through the heat-treated region, which was processed with 6 pulses from a 10 mm diameter at 6 MeV, 0.9 kA/pulse operating at 2 kHz PRF. These conditions led to an average surface fluence of 21 J/mm^2 in the interacted region, which heat-treated the steel without melting. The heat treated region, which etches darker than the base material, is elliptical in cross section and is centered below the surface of the plate. This unique shape of the heat treated region indicates that the beam internally heated the steel, and the center of the heat treated-region is located approximately 1 mm below the surface of the plate. The diameter of the heat-treated region is approximately 9 mm, which is similar to the diameter of the beam, and there exists evidence of heat treating to a depth of approximately 2 mm below the surface of the plate.

A Monte Carlo model of the energy deposition in steel is shown in Fig. 2b for a single 10 mm diameter electron beam pulse at 6 MeV, 0.9 kA, and 50 ns pulse duration. The Monte Carlo simulated beam conditions were the same as those used to process the plain carbon steel sample, and the depth-dose profile indicates that the overall contours match the general shape of the heat treated zone. For a single pulse, the peak energy dose was calculated to be 160 J/g; multiplying this value by the total number of pulses received by the sample (six) gives a dose of 960 J/g, which corresponds to the highest dose received by the sample, assuming no heat diffusion during the multiple pulse processing.

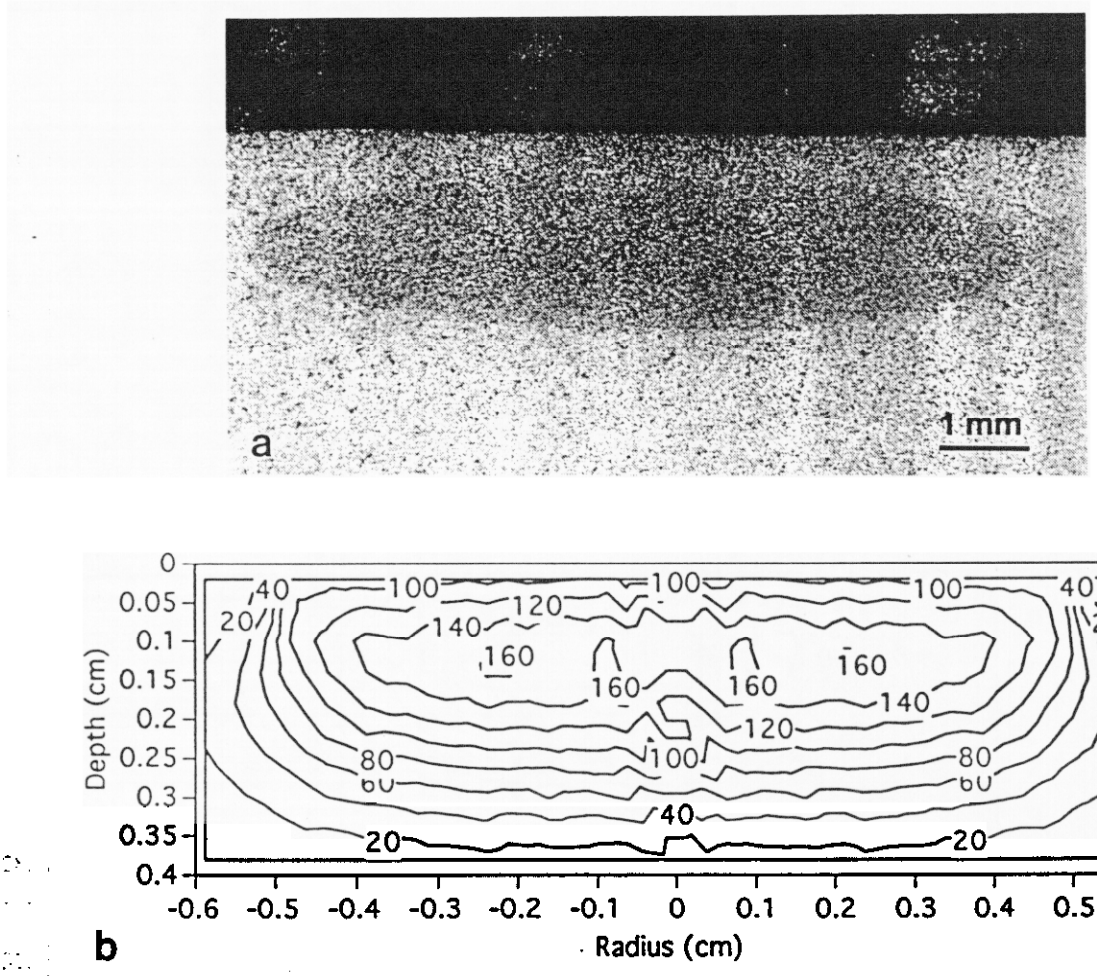

Fig. 2: a) A subsurface heat-treated zone in plain carbon steel produced at a fluence of 21 J/mm^2 from 6 pulses of a 6MeV, 50 ns, 0.9 kA/pulse, 10 mm diameter beam. b) CYLTRAN Monte Carlo calculations of the energy deposition in steel for a single pulse of the above parameters. The contours are given in J/g.

Figure 3a shows a metallographic cross section through a region of a steel plate that was processed with a fluence of 95 J/mm^2 from 10 pulses with a 6 mm diameter, 6 MeV, 0.9 kA/pulse beam operating at 2 kHz PRF. After processing, the plate showed signs of surface swelling, and a metallographic section was taken through the center of the dimple that appeared on the surface of the plate. The metallographic cross section revealed a subsurface molten zone surrounding a vapor cavity. The presence of the subsurface void explains the dimple that was observed on the surface of the plate, which formed from the pressure that developed within the vapor cavity expanded to deform the surface of the plate.

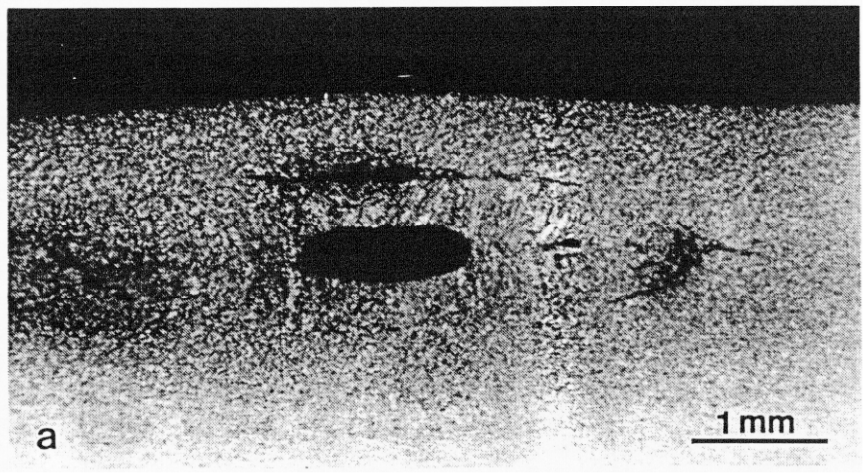

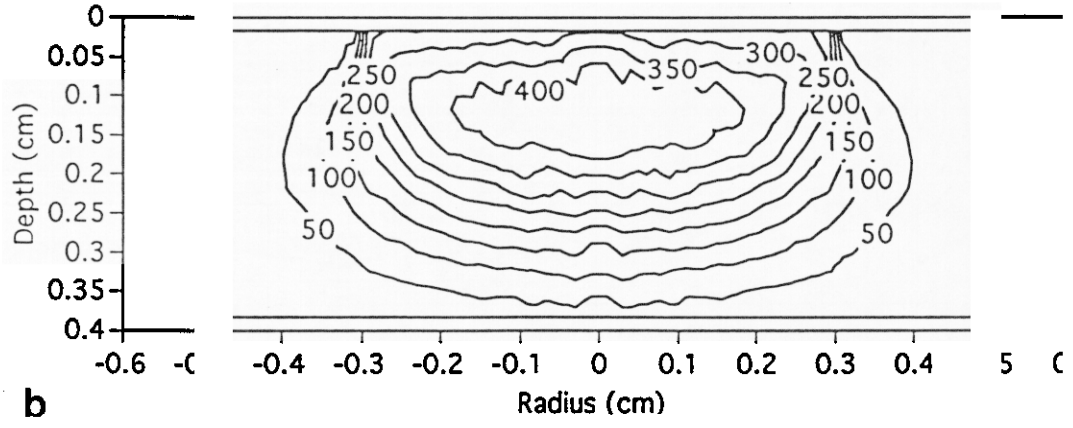

Fig. 3: a) A subsurface heat-treated zone in plain carbon steel produced at a fluence of 9 J/mm^2 from a 6 MeV, 50 ns, 0.9 kA/pulse, 6 mm diameter beam. b) CYLTRAN Monte Carlo calculations of the energy deposition in steel for a single pulse of the above parameters. The contours are given in J/g.

A Monte Carlo model of the energy deposition in steel is shown in Fig. 3b for a single 6 mm diameter electron beam pulse operating at 6 MeV, 0.9 kA, and 50 ns pulse duration. The Monte Carlo simulated beam conditions were the same as those used to process the plain carbon steel sample, and the depth-dose profile again indicates that the overall contours match the general shape of the heat treated zone. For a single pulse, the peak energy dose was calculated to be 400 J/g; multiplying this value by the total numbe of pulses received by the sample (ten) gives a dose of 4000 J/g, which corresponds to the highest dose received by the sample, assuming no heat diffusion during the multiple pulse processing.

Estimating the Peak Dose Delivered by HEEBs

The peak dose delivered by HEEBs is approximately a linear function of energy fluence on the surface of the sample, as long as the beam diameter and voltage are held constant. Therefore, the depth-dose profile of a single Monte Carlo calculation can be linearly scaled to predict the depth-dose profile for different beam currents, pulse durations, and total number of pulses. The principal assumption that is made here is that heat diffusion that occurs between the first and last pulses does not significantly affect the energy distribution within the sample, and this assumption is reasonable for a sample that is processed with less than 10 pulses at kHz PRFs.

However, the depth-dose relationship does not necessarily scale with average surface fluence for different beam diameters, since scattering of the electrons within the material may lead to different energy distributions. The "range" of a 6 MeV electron in steel (i.e. the average length of the rather tortuous path that the electron follows as it slows down from an initial energy of 6 MeV and, after undergoing many elastic and inelastic scattering collisions, finally comes to rest in the material) is approximately 5 mm. Therefore, electrons will be quickly scattered outside the diameter of those beams having diameters less than (or comparable to) the electron's range, and the energy deposition profile in the material will reflect this scattering. This effect is less important in electron beams with diameters many times larger than the electron range in the material, in which case the scattered electrons have a much higher probability of continued residence within the beam body as it traverses the material. In these cases, a noticeable "buildup" of energy deposition below the surface is observed, as shown in Figs. 2 and 3.

Similarly, if the beam voltage is changed, the electrons do not penetrate as deeply and a different depth-dose profile results. Since an electron's range (and its net penetration depth below the surface of the workpiece) is approximately a linear function of energy between 1-10 MeV [2], one has a flexible "knob" on increasing or decreasing the depth of the heat treatment by increasing or decreasing the accelerated electron beam's kinetic energy [7].

Monte Carlo simulations of depth-dose profiles in steel were made for a geometric progression of beam diameters, between 2 and 44 mm, in order to determine the influence of beam diameter on the depth-dose profile and the magnitude of the peak dose for a 6 MeV, 1 kA/pulse, 50 ns beam (300 J/pulse). For each beam diameter, the peak dose and the depth of the peak dose below the surface were determined and are plotted in Fig. 4. The results show that the location of the peak dose is 1.25 mm below the surface of the plate and constant for beam diameters greater than 5 mm (this diameter is approximately equal to the electron range in steel); for smaller beam diameters, the depth of the peak dose decreases, indicating that the peak dose is located closer to the surface of the plate. This figure also shows that the magnitude of the peak dose decreases from 3000 J/g to less than 10 J/g, as the beam diameter increases from 2 to 44 mm. Figure 5 re-plots the peak dose as a function of average surface fluence rather than beam diameter, in an attempt to linearize the peak dose relationship. At low fluence, <15

J/mm^2, the peak dose increases linearly with fluence. This linear regime is valid for beam diameters greater than 5 mm. However, at higher fluence, >15 J/mm^2, the peak dose increases with beam fluence, but at a decreasing rate.

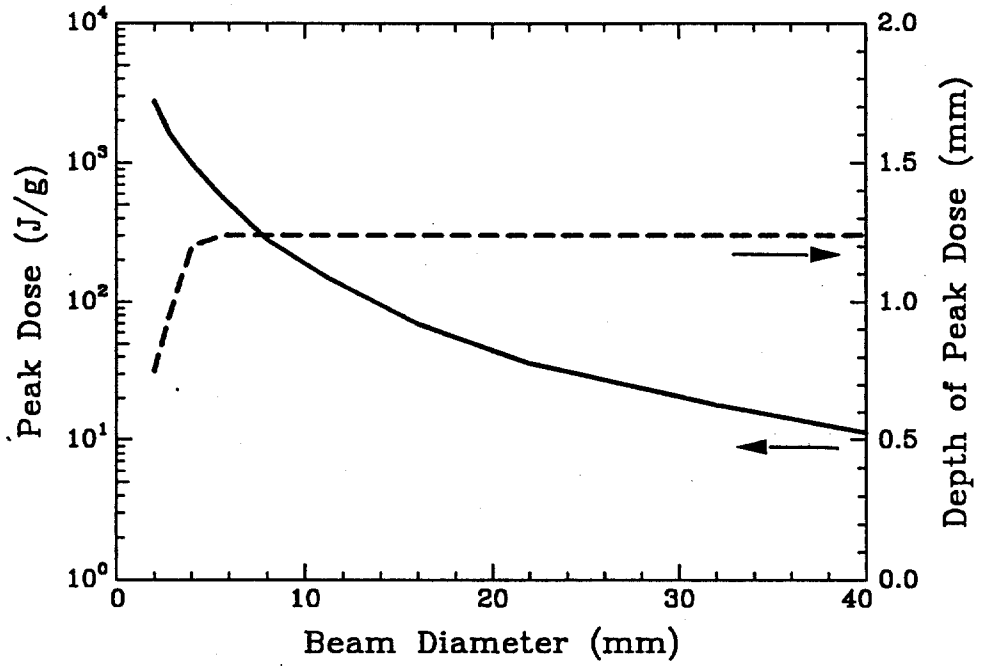

Fig. 4: Peak dose (solid line) and depth of the peak dose (dashed line) in steel plotted as a function of beam diameter for a 6 MeV beam operating at 300 J/pulse.

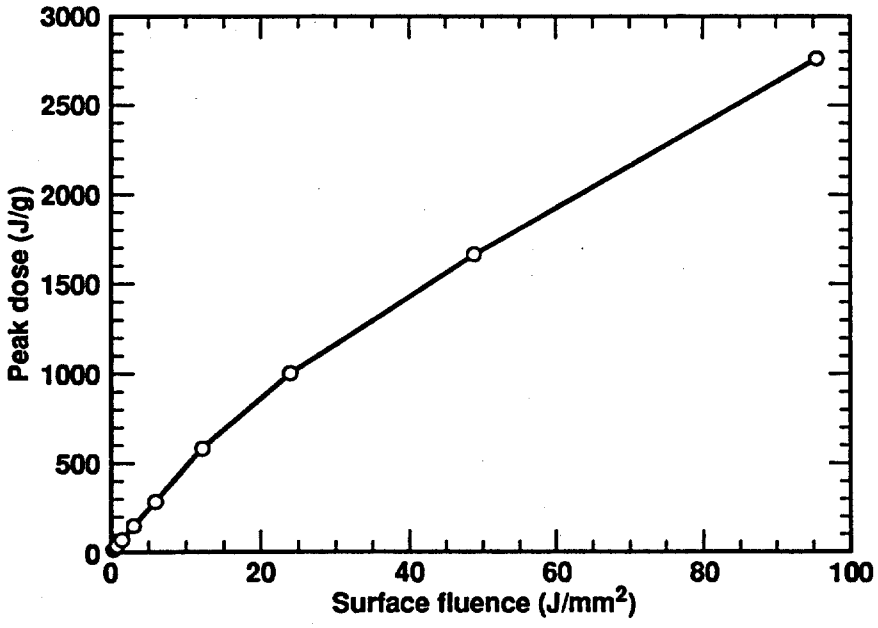

Fig. 5: Relationship between peak dose in steel and beam fluence, for beam diameters between 2 and 44 mm from a single pulse at 6 MeV, 50 ns, 1.0 kA/pulse.

Typical heat treating conditions require the beam to be spread out over relatively large areas for efficient processing of materials. Under these conditions, the beam diameter will be greater than 5 mm and the linear relationship between the peak dose and the surface fluence will hold. For a 6 MeV, 1 kA/pulse beam with a diameter greater than 5 mm, the peak dose can be estimated using the following relationship :

$$D^* = 46.8\ \Phi \qquad (eq.1)$$

where D* is the peak dose in J/g and Φ is the surface fluence measured in J/mm^2.

This first order approximation for the peak dose can be used to predict the peak temperature, the phase transitions, and the peak heating rate in steel, as discussed in the following sections. Moreover, since the depth of the peak dose does not change for diameters greater than 5 mm, and since the diameter of the heated region is approximately the same as the beam diameter, the size and shape of the heat treated zone can also be estimated for 6 MeV electron beam processing of steel.

Calculating Peak Temperatures

In order to heat treat steel without melting, the sample must be heated to a temperature between the austenite solution temperature and the melting point of the alloy. Therefore, it is necessary to convert the depth-dose profiles generated by the Monte Carlo calculations into a temperature rise in the sample in order to predict the influence of processing parameters on the resulting microstructure. Correlating the dose given to steel with its temperature rise requires the heat capacity of the steel and the enthalpy of any phase transitions that occur. Phase transition enthalpies $\Delta H_{\alpha-\gamma}$, $\Delta H_{\gamma-\delta}$, $\Delta H_{\delta-L}$ and ΔH_{L-v}, correspond to the bcc-to-fcc, fcc-to-bcc, bcc-to-liquid, and liquid-to-vapor, phase transitions respectively, and are summarized in Table 1 [8], while the coefficients, a and b, of the temperature-dependent heat capacity ($C_P(T)$) of these phases are given in Table 2 for the relationship $C_P(T)=a+bT$ [9]. Within a given phase, the temperature-dose relationship was determined using the following equation:

$$D = \int_{To}^{T_f} C_p\ (T)dT \qquad (eq.2)$$

where D is the dose given to the sample, T is the temperature, To is the initial temperature, and T_f is the final temperature after processing. The enthalpy of transformation is further added to the required dose at each of the phase transformation temperatures.

Table 1: Phase transition enthalpies of iron.

Parameter	$\Delta H_{\alpha-\gamma}$	$\Delta H_{\gamma-\delta}$	$\Delta H_{\delta-L}$	ΔH_{L-v}
T (^{o}C)	914	1401	1536	2730
Dose (J/g)	16	11	289	6330

Table 2: Coefficients for the temperature-dependent heat capacity of iron.

Parameter	Fe_{bcc}	Fe_{fcc}	Fe_{L}
a (J/gK)	0.664	0.438	0.749
b (J/gK^2)	0.110×10^{-3}	0.151×10^{-3}	-

Figure 6 plots the temperature-dose relationship for iron, as calculated from the data presented in Tables 1 and 2. This figure indicates that the minimum dose required to bring iron to the austenite temperature (914^{o}C) is 626 J/g, with an additional 16 J/g required to austenitize iron at this temperature; the minimum dose to bring iron to its melting point (1536^{o}C) is 1050 J/g, with an additional 289 J/g required to melt iron at this temperature; and the minimum dose to bring iron to its vaporization temperature (2730^{o}C) is 2230 J/g, with an additional 6630 J/g required to vaporize iron at this temperature. For plain carbon steel containing 0.16%C, the austenitizing and melting temperatures will be lower than that of pure iron (878^{o}C and 1521^{o}C respectively).

The peak temperature received by the processed samples can be estimated using the temperature-dose relationship. For the sample shown in Fig. 2a, the peak dose was calculated to be 960 J/g, which corresponds to a peak temperature of 1400^{o}C. This temperature is above the austenite temperature and below the melting temperature of this alloy, and is in the heat treating temperature range for steel. The experimental results confirm these calculations, and show that the sample was heat treated without any evidence of melting, with a subsurface peak in energy approximately 1 mm below the surface of the plate. For the sample shown in Fig. 3a, the peak dose was calculated to be 4000 J/g, which exceeds the dose required to bring steel to its vaporization temperature (2250 J/g) but is insufficient to completely vaporize the sample (8580 J/g). The peak temperature of this sample is equal to the vaporization temperature of 2730^{o}C, which was achieved prior to the completion of processing. The experimental results also confirm these calculations, and show that the sample was melted and partially vaporized with a subsurface peak in energy also occurring approximately 1 mm below the surface of the plate.

Therefore, the Monte Carlo calculations appear to correlate well with the HEEB processed steel in terms of the predicted peak dose, depth-dose profile, and overall distribution of energy deposited in the processed sample. This good correlation between the experiments and the calculations indicates that the Monte Carlo code can be used to estimate the beam processing parameters, i.e., beam diameter, beam energy, beam fluence etc., for producing desired metallurgical modifications to steel. In addition, this computational method can be used as an inexpensive method for predicting the interaction of HEEBs with materials that have different thermophysical properties than steel, thus allowing processing parameter windows to be defined prior to performing the actual HEEB processing experiments.

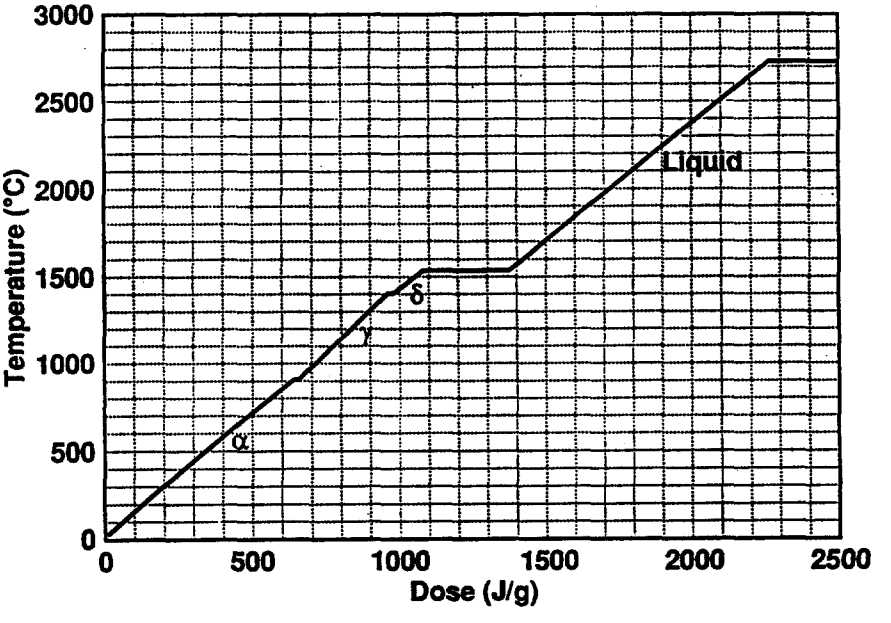

Fig. 6: Temperature-dose relationship for iron.

Calculating Peak Heating Rates

The peak dose and peak temperature can be calculated for HEEB processed steel using the relationships presented in the preceding section. From this information, the peak heating rate can easily be calculated using the relationship:

$$\varepsilon = \frac{\Delta T}{\Delta t} \qquad (eq.3)$$

where ε is the heating rate, ΔT is the temperature rise in the steel (as determined from Fig. 6), and Δt is the difference in time between the first and last pulse. For a single pulse, Δt is equal to the pulse duration (~50 ns), which leads to exceptionally high heating rates, which are on the order of 10^9 to 10^{10} °C/s.

The peak heating rates for the sample shown in Fig. 2 can be estimated from the peak dose of 960 J/g received by the sample, which corresponds to a temperature rise of 1400°C. This rise in temperature occurred over 6 pulses at 2 kHz PRF, which corresponds to a 0.0025 s difference in time between the first and the last pulse. From eq. 3, the peak heating rate for the sample can be calculated to be 5.6×10^5 °C/s. Similar calculations for the sample shown in Fig. 3, which reached the vaporization temperature in approximately 6 pulses (the remainder of the 10 pulses only served to partially vaporize the sample at the vaporization temperature), show that this sample was heated at a rate of approximately 1.1×10^6 °C/s.

The heating rate can be controlled over several orders of magnitude through variations in the beam intensity and the pulse repetition frequency. Figure 7 plots the calculated heating rate for a 6 MeV, 300 J/pulse beam as a function of surface fluence, for a 1200 °C temperature rise in steel (total surface fluence of 18 J/mm^2). In this figure, the heating rate is shown for multiple pulse spot processing of steel at two different PRFs of 100 Hz and 2000 Hz. At 2000 Hz, peak heating rates higher than 10^6 °C/s can be achieved, while at 100 Hz, heating rates as low as $<10^4$ °C/s can be produced and by decreasing the intensity of the heat source, which requires more pulses to reach the desired temperature. These heating rates are many orders of magnitude greater than can be produced by conventional heat sources, and because of the deep penetration of the high energy electrons into steel, these beams have the additional advantage of being able to transformation harden steel to a depth of approximately 2 mm without overheating and melting the surface.

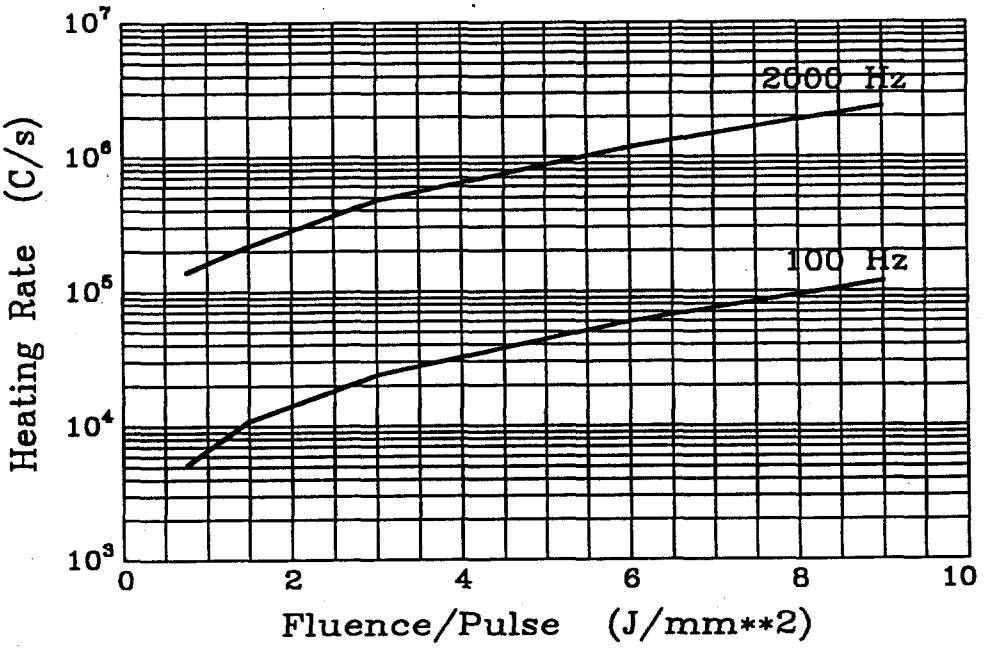

Fig. 7: Peak heating rate for a 1200 °C temperature rise in iron as a function of fluence/pulse, at two PRFs of 100 and 2000 Hz.

CONCLUSIONS

1. The interaction of a stationary 6 MeV pulsed electron beam with a plain carbon steel plate showed that a beam fluence of approximately 20 J/mm^2 will transformation harden the steel without melting, while a beam fluence of approximately 100 J/mm^2 will cause subsurface melting and vaporization to occur. In both cases, the experiments showed that the peak energy deposition occurs approximately 1 mm below the surface of the processed plate.

2. Monte Carlo calculations were used to simulate the HEEB/material interaction in steel. The results of these calculations correlated well with experiments performed on the ETA II accelerator, and can be used to predict the depth-dose profile and the location of the peak energy dose for a wide range of processing conditions.

3. A series of Monte Carlo calculations for a 6 MeV, 1 kA/pulse, 50 ns beam with a range of beam diameters showed that the peak dose deposited in steel increases linearly with beam fluence up to a fluence of 15 J/mm^2 (beam diameters larger than 5 mm). For higher fluence (beam diameters less than 5 mm), the peak dose deviates from linearity. These calculations further showed that the peak dose occurs 1.25 mm below the surface of the steel for beam diameters greater than 5 mm, and slightly closer to the surface of the steel for beam diameters smaller than 5 mm.

4. The peak temperature, peak heating rate, and the phase transformations that occur in HEEB processed steel can be calculated using the relationships presented in this paper. These relationships can be used to predict the influence of beam diameter, number of pulses, and energy per pulse on the phase transformation characteristics of steel, but are only valid for a 6 MeV beam.

ACKNOWLEDGMENTS

The authors would like to acknowledge the support of Don Prosnitz for providing access to the ETAII accelerator, Bob Kershaw for optical metallography, Skip Fields and Scott Hulsey for operation of the electron beam accelerator, and Cliff Holmes and Don Hathaway for sample preparation. This work was performed under the auspices of the U. S. Department of Energy, Lawrence Livermore National Laboratory, under Contract No. W-7405-ENG-48.

REFERENCES

1. F. Roozeboom and N. Parekh, "Rapid Thermal Processing Systems: A Review With Emphasis on Temperature Control," J. Vac. Sci. Technol. B 8 (6), p. 1249, Nov/Dec 1990.

2. A. C. Smith, Jr. , E. E. Nolting and W. M. Fawley, " An Overview of High Energy Electron Beam Science," presented at the AWS sponsored conference on *High Energy Electron Beam Processing of Materials*, held in Cambridge, Massachusetts, September, 1992.

3. J. W. Elmer, M. A. Newton and A. C. Smith Jr., "Transformation Hardening of Steels Using High Energy Electron Beams," submitted to the *Welding Journal*, October, 1993.

4. Y. P. Chong, F. J. Deadrick, D. G. Hirzel, J. S. Kallman, P. Lee, J. P. Poulter, W. E. Rivera, P. L. Stephan, and J. T. Weir, Optical Cerenkov Measurements of Emittance Growth in the ATA Beam Under Laser Ion-Guiding," UCRL 99782, prepared for the 1989 Particle Accelerator Conference, Chicago, Ill, March 20-23, 1989.

5 *ITS Version 3.0: The Integrated TIGER Series of Coupled Electron/Photon Monte Carlo Transport Codes*, J. A. Halbleib, et al., Sandia National Laboratories Report SAND91-1634, UC-405, March 1962.

6. *Monte Carlo Transport of Electrons and Photons*, editors T. M. Jenkins, W. R. Nelson and A. Rindi, Plenum Press, 1988.

7. *Physics of Nuclei and Particles,* by P. Marmier and E. Sheldon, Academic Press, New York, 1969.

8. *Handbook of Chemistry and Physics, 54th edition,* CRC Press, 1974.

9. *Metallurgical Thermochemistry, 5th edition,* by O. Kubaschewski and C. B. Alcock, published by Pergamon Press, 1979.

Technical Information Department • **Lawrence Livermore National Laboratory**
University of California • Livermore, California 94551